Molecular simulation of crystal nucleation in n-octane melts

Massachusetts Institute of Technology

Molecular Simulation of Crystal Nucleation in *n*-Octane Melts

Peng Yi （易鹏）[1], Gregory C. Rutledge[2]

[1]*Department of Physics and* [2]*Department of Chemical Engineering*

Massachusetts Institute of Technology, Cambridge, Massachusetts 02139, USA

Homogeneous nucleation of the crystal phase in *n*-octane melts was studied by molecular simulation with a realistic, united-atom model for *n*-octane. The structure of the crystal phase and the melting point of *n*-octane were determined through molecular dynamics simulation and found to agree with experimental results. Molecular dynamics simulations were performed to observe the nucleation events at constant pressure and constant temperature corresponding to about 20% supercooling. Umbrella sampling Monte Carlo simulations were used to calculate the nucleation free energy for three temperatures, ranging from 8% to 20% supercooling, and to reveal details of the critical nucleus for the first time. The cylindrical nucleus model was found to provide a better quantitative description of the critical nucleus than the spherical nucleus model. The interfacial free energies of the cylinder model were calculated from the simulation data. As the temperature increased, the interfacial free energy of the side surface remained relatively unchanged, at 7 to 8 mJ/m^2, whereas the interfacial free energy of the end surface decreased significantly from 5.4 mJ/m^2 to about 3 mJ/m^2. These results, and the methods employed, provide valuable and quantitative information regarding the rate limiting step during the solidification of chain molecules, with ramifications for both short alkanes and polymers.

I. INTRODUCTION

One of the most important phenomena in molecular systems is nucleation of the crystal phase from a homogeneous melt. It is generally the rate-limiting step in the transformation from an amorphous liquid phase to an ordered solid phase, and is fundamental to understanding the kinetics of this phase transition. Although it has been the subject of extensive experimental and theoretical study for decades,[1,2] many aspects of the microscopic mechanism of homogeneous crystal nucleation remain poorly understood, including the rate of formation of the crystal phase, structure and composition of the embryonic crystal nuclei, etc. This problem is especially severe for chain molecules, due to their strong anisotropy and their conformational flexibility. Homogeneous nucleation of a crystal phase of chain molecules from the melt is particularly complex because the ordering of chains or segments of chains is slowed by viscous effects and the multiplicity of conformational states of the chains. Therefore, even under quiescent conditions, the microscopic mechanisms of chain molecule crystallization remain a subject of debate.[3] For sufficiently long chains and polymers, crystallization is further complicated by entanglement, and the molecules participate in the crystal phase only partially, resulting in the so-called "semicrystalline" state. Nevertheless, semicrystalline polymers account for the largest volume of commercially available polymer. Therefore, understanding the mechanism of crystal nucleation of chain molecules is important not only to

fundamental understanding of this phase transition but also to development of industrial applications.

The key problem in the study of homogeneous crystal nucleation is to identify the critical nucleus. Not only is the formation of the critical nucleus the rate-limiting step in the overall crystallization process, but the structure of the critical nucleus serves as the base for the subsequent growth of the crystallite into a new phase. In the case of chain molecules, experiments have been instrumental in resolving complex crystal structures[4] and detecting the onset of crystallization under quiescent conditions or mechanical perturbation[5-8], but for the study of the critical nucleus only computer simulations provide the necessary resolution to understand the sequence of events at the molecular level that give rise to crystallization.

In several previous molecular dynamics simulation studies, crystallization has been observed, and the structure of the final crystalline phase has been analyzed.[9,10] However, the critical nucleation event was never clearly identified in any of these studies. The induction period, which is a characteristic feature of nucleation, and the growth period often could not be clearly distinguished. This is probably due to the exceptional rigidity of the chain models often adopted, which artificially accelerates crystallization for the purpose of observation on the simulation time scale. Rigid chains have substantially higher melting temperatures and exhibit different kinetics of crystallization from those of semi-flexible chains.[11] Meanwhile, robust simulation methods have been developed and applied to study the critical nucleus in relatively

simple systems like the Ising model, the Lennard-Jones model, the hard-sphere model, and water vapor.[12-16] However, to our knowledge, none of these methods has been used to investigate the nucleation event during crystallization from a homogeneous melt in a chain molecule system.

In this work, we use molecular simulation and a realistic, semi-flexible alkane model to study primary crystal nucleation of the short-chain molecule *n*-octane from the homogeneous melt. Specifically, we identify for the first time the critical nucleus of *n*-octane, examine the structure and free energy of the critical nucleus, and use these to discriminate between several simplified nucleus models. Both molecular dynamics and Monte Carlo methods are employed, and their results compared. The *n*-octane system was chosen because it has no rotator phase[17] to complicate the interpretation of the phase transition, and because it is known to crystallize on a time scale accessible by molecular dynamics simulation.

II. Theory

Classical nucleation theory (CNT)[1] has been widely used to describe homogeneous nucleation. According to CNT, a crystal nucleus consisting of the thermodynamically most stable phase is separated from the surrounding liquid by a sharp, infinitely thin interface. For temperatures below the melting point, the competition between the free energy gain of the interior of the nucleus and the free energy cost of the interface creates a free energy barrier. The time required to

surmount this free energy barrier results in the observed induction period before a nucleation event.

According to CNT, for a spherical nucleus of radius R, the free energy of formation ΔG can be written as

$$\Delta G = 4\pi R^2 \sigma - \frac{4\pi R^3}{3}\Delta G_v,$$ (1)

where σ is the crystal-liquid interfacial free energy per unit area and ΔG_v is the Gibbs free energy difference per unit volume between the liquid and crystal phases at the same temperature. Eq. (1) can be rewritten in terms of nucleus size n as

$$\Delta G = (36\pi)^{1/3}\left(\frac{n}{\rho_n}\right)^{2/3}\sigma - n\Delta G_m,$$ (2)

where nucleus size n is the number of molecules in the nucleus, ρ_n is the molecule number density of the crystal phase, and

$$\Delta G_m = \Delta G_v / \rho_n$$ (3)

is the Gibbs free energy difference per molecule.

For a small degree of supercooling, ΔG_m can be expressed as

$$\Delta G_m \approx \Delta H_f \Delta T / T_m,$$ (4)

where ΔH_f is the heat of fusion per molecule at the equilibrium melting temperature T_m, and ΔT (equal to $T_m - T$) is the degree of supercooling.

The free energy of formation for the critical nucleus is the critical free energy, ΔG^*, and is obtained by finding the maximum in ΔG with respect to nucleus size n in Eq. (2):

$$\Delta G^* = \frac{16\pi}{3} \frac{\sigma^3}{(\Delta H_f \Delta T \rho_n / T_m)^2} \tag{5}$$

Correspondingly, the size of the critical nucleus for the spherical nucleus model is

$$n^* = \frac{32\pi}{3\rho_n^2} \left(\frac{\sigma}{\Delta H_f \Delta T / T_m} \right)^3 \tag{6}$$

For crystal nucleation of chain molecules, a cylindrical nucleus model might be more suitable.[6-8] This model distinguishes two types of surface: the chain-end surface and the chain-side or lateral surface. The free energy of formation of a cylindrical nucleus with radius r and length l can be written as

$$\Delta G = 2\pi r^2 \sigma_e + 2\pi r l \sigma_s - \pi r^2 l \Delta G_v , \tag{7}$$

where σ_e and σ_s are the crystal-liquid interfacial free energies per unit area for the end surface and the side surface, respectively. If both the radius and the length of the cylinder vary, the critical free energy ΔG^* is

$$\Delta G^* = 8\pi \frac{\sigma_s^2 \sigma_e}{(\rho_n \Delta H_f \Delta T / T_m)^2} , \tag{8}$$

and the critical nucleus has length l^* and radius r^* given by

$$l^* = 4\sigma_e T_m / (\rho_n \Delta H_f \Delta T) \tag{9a}$$

and

$$r^* = 2\sigma_s T_m / (\rho_n \Delta H_f \Delta T), \tag{9b}$$

respectively. Thus the critical nucleus size n^* for the cylindrical nucleus model of variable length is

$$n^* = 16\pi \frac{\sigma_s^2 \sigma_e}{\rho_n^2 (\Delta H_f \Delta T / T_m)^3}. \tag{10}$$

For both the spherical and cylindrical nucleus models, a simple relation exists between the critical size n^* and the critical free energy ΔG^*:

$$n^* = \frac{2\rho_n}{\Delta H_f \Delta T / T_m} \Delta G^*. \tag{11}$$

Eq. (11) can be used to examine the spherical model and the cylindrical model of variable length.

For short-chain molecules, the critical cylinder length l^* can be greater than the length of the respective chain molecule length l_0. In this case, a more appropriate model for the cylindrical nucleus may be one in which the length of the critical nucleus is fixed and equal to l_0. In this model, the free energy of formation is expressed as

$$\Delta G = 2\pi r^2 \sigma_e + 2\pi r l_0 \sigma_s - \pi r^2 l_0 \Delta G_v \tag{12}$$

or, in terms of nucleus size n,

$$\Delta G = \frac{2n}{l_0 \rho_n} \sigma_e + 2\sqrt{\frac{\pi l_0 n}{\rho_n}} \sigma_s - n\Delta G_m. \tag{13}$$

Thus, by finding the maximum of ΔG with respect to n in Eq.(13), the critical free energy for the cylindrical nucleus model of fixed length is found to be

$$\Delta G^* = \frac{\pi l_0^2 \sigma_s^2}{(l_0 \rho_n \Delta H_f \Delta T / T_m - 2\sigma_e)} \tag{14}$$

and the critical nucleus size is

$$n^* = \frac{\pi l_0^3 \rho_n \sigma_s^2}{(l_0 \rho_n \Delta H_f \Delta T / T_m - 2\sigma_e)^2} \cdot \tag{15}$$

Conversely, if the values of ΔG^* and n^* are known, then the interfacial free energies can be calculated from

$$\sigma_s = \sqrt{\frac{\rho_n}{\pi l_0} \frac{\Delta G^{*2}}{n^*}} \tag{16a}$$

and

$$\sigma_e = \frac{l_0 \rho_n}{2} \left(\frac{\Delta H_f \Delta T}{T_m} - \frac{\Delta G^*}{n^*} \right). \tag{16b}$$

According to transition state theory, the nucleation rate I is given by

$$I = I_0 e^{-\Delta G^* / k_B T}, \tag{17}$$

where I_0 is a kinetic prefactor, and k_B is the Boltzmann factor. I_0 is given as

$$I_0 \approx N_v^0 v, \tag{18}$$

where N_v^0 is the molecule number density in the melt state, and v is the frequency of molecular transport at the nucleus surface. Furthermore, v can be approximated using the Stokes-Einstein relation

$$v \approx k_B T / 3\pi a_0^3 \eta, \tag{19}$$

where a_0 is the molecular diameter and η is the viscosity.[8] The critical free energy ΔG^* can therefore be calculated directly from Eq.(17) if I, I_0 and T are known,[8] or

from the temperature dependence of the nucleation rate I, assuming that I_0 is only weakly temperature-dependent compared to $\Delta G^*/k_B T$ [7]. These two methods are usually used to calculate the interfacial free energy from the experimentally measured nucleation rate. However, these methods provide only ΔG^*, from which only a single measure of the interfacial free energy of a nucleus can be calculated, e.g., σ in the spherical nucleus model, or $\sigma_s^2 \sigma_e$ in the variable-length cylindrical nucleus model. In order to calculate σ_s and σ_e separately, the structure of the critical nucleus (i.e. its size and shape) are needed, in addition to ΔG^*.

III. Method

A. *System*. We simulated a system containing either 480 or 960 *n*-octane chains using the isothermal-isobaric (*NPT*) ensemble with the pressure P set at 1 atm. Simulations in which the crystal phase spanned one or more dimensions of the simulation box were conducted with fully variable side lengths and angles of the simulation box; for all other simulations, the angles were fixed at 90° and only the side lengths were allowed to vary independently. Periodic boundary conditions were employed in all three directions.

B. *Force Field.* We used a united-atom (UA) force field proposed originally by Paul, Yoon, and Smith[18] and modified subsequently by Waheed *et al.*[19,20], designated PYS. This force field was parameterized using experimental data and quantum calculations on short alkanes and has been shown to describe polyethylene melts accurately.[18,21]

In this force field, polyethylene and alkane chains are composed of spherical beads, or "united atoms," each representing a CH_2 group (or CH_3 for the terminal beads). CH_2 and CH_3 beads differ only in mass. Each bead interacts through bonded and nonbonded potentials. The bond stretching potential between two adjacent beads is

$$E_{bond} = k_l \times (l - l_0)^2 , \tag{20}$$

where l is the length of bond, k_l is the bond stretching constant, which is equal to 1.46×10^5 kJ/mol/nm^2, and l_0 is 0.153 nm. The bond angle bending potential among three adjacent beads is

$$E_{angle} = k_\theta \times (\theta - \theta_0)^2 , \tag{21}$$

where θ is the complement of the bond angle, k_θ is the angle bending constant, which is 251.04 kJ/mol/rad^2, and θ_0 is 1.187 rad. The bond torsion potential among four adjacent beads is

$$E_{torsion} = \frac{1}{2}\left[k_1 \times (1 - \cos\varphi) + k_2 \times (1 - \cos 2\varphi) + k_3 \times (1 - \cos 3\varphi)\right], \tag{22}$$

where φ is the torsion angle, the torsion constant k_1 is 6.78 kJ/mol, k_2 is -3.60 kJ/mol, and k_3 is 13.56 kJ/mol.

The nonbonded interactions are described by a Lennard-Jones 12-6 potential for all intermolecular interactions between beads on different chains and for intramolecular interactions between beads on the same chain that are separated by four or more bonds,

$$E_{LJ} = 4\varepsilon \left[\left(\frac{\sigma}{r} \right)^{12} - \left(\frac{\sigma}{r} \right)^{6} \right], \tag{23}$$

where ε is 0.39 kJ/mol, and σ is 0.401 nm. The Lennard-Jones potential was truncated at 2.5σ, and tail corrections were added for potential energy and pressure that assume the radial distribution function $g(r) = 1$ beyond this cutoff.

C. *Molecular Dynamics Simulation.* Molecular dynamics (MD) simulations are suitable for obtaining a direct, unbiased, kinetic description of the nucleation process for small molecules at moderate to large supercooling. However, for large molecules or small supercooling, if the critical free energy of nucleation is too high, the spontaneous crossing of the free energy barrier becomes very unlikely, and nucleation cannot be observed in the timescale accessible by brute-force MD simulations.

We carried out MD simulations using open source code for the DL_POLY package [22] and the LAMMPS (Large-scale Atomic/Molecular Massively Parallel Simulator) package.[23] The DL_POLY package was used for simulations to determine the crystal structure, melting point and heat of fusion of *n*-octane, where independent variation of the box angles was required; for all other MD simulations, LAMMPS was used. In the MD simulations, the initial velocities of all beads were generated from the Maxwell-Boltzmann distribution according to the desired temperature, and the equations of motion were integrated using the velocity Verlet method with an

integration time step Δt equal to 2fs. Waheed *et al.*[19] and Lavine *et al.*[24] have previously evaluated the effect of the integration time step during the MD simulation of *n*-alkanes with this PYS force field. They found that changing Δt from 1 fs to 5 fs increased the bond energy, the angle-bending energy, and the relaxation time for the chain-orientation autocorrelation function by approximately 10%. The consequence of these errors was mitigated through the use of a thermostat, such that no detectable difference in crystallization kinetics was observed for simulations with Δt between 1 and 5 fs.

For a reaction coordinate to characterize crystallization, we monitored the size of the *largest* crystal nucleus in the system, n_{max}, during the simulation. This choice was made because the dynamics of the nucleation process is dominated by the biggest nucleus in the system.[15] In calculating the nucleus sizes n, we adopted the definition of nucleus used by Esselink:[10] if two chain molecules have the same orientation and are neighbors, then they belong to the same nucleus. They are considered to have the same orientation if the angle between their main axes is less than or equal to 10 degrees, and they are neighbors if their centers of mass are less than or equal to 1.5σ apart. The main axis of a molecule is the principal axis with the smallest moment of inertia. By this definition, one molecule is either part of the nucleus or not; it cannot be "partially crystalline." Because the PYS force field predicts a persistence length of about 0.8 nm,[25] which is comparable to the extended length of one *n*-octane chain, 0.82 nm, assuming that every chain of *n*-octane joins the crystal as a whole, rather in segments, is reasonable.

In addition to n_{max}, two other variables that measure the order of the system were monitored. The first variable is the global orientation order parameter, P_2, which is defined as

$$P_2 = \left\langle \frac{3\cos^2\theta_{ij} - 1}{2} \right\rangle_{i,j\neq i},\tag{24}$$

where θ_{ij} is the angle between the vector from the $(i-1)^{th}$ bead to the $(i+1)^{th}$ bead, and the vector from the $(j-1)^{th}$ bead to the $(j+1)^{th}$ bead. The average is taken over all pairs of chords and over all molecules. The second variable is the fraction of torsions in the *trans* state in the system, P_{trans}. A *trans* state for a torsion angle is defined as a state in which the torsion angle is between -60° and +60°. P_2 and P_{trans} are standard measures of the global order in a chain molecule system. In comparison, n_{max} is a measure of the local order.

Several methods have been developed to estimate the critical nucleus size n^* from MD simulations.[13,16] These methods are presented in different ways, but they are interrelated.[26] The approach by Wedekind *et al.*[16] makes particularly clear the link between the classical theoretical treatment and the quantities available by MD simulation, and was employed here. According to this method, as long as the critical free energy is relatively high ($\Delta G^* \gg k_B T$), the mean first passage time (MFPT) of the maximum nucleus size, $\tau(n_{max})$, takes the form

$$\tau(n_{max}) = 0.5\tau^* \left[1 + erf(b \times (n_{max} - n^*))\right],\tag{25}$$

where τ^* is the average induction time, b characterizes the curvature at the top of the free energy barrier, and n^* is the critical nucleus size. This method allows us to estimate n^*, b, and τ^* from MD simulations.

D. *Monte Carlo Simulation*. Nucleation at small supercooling is not accessible by brute-force MD simulation because of the high free-energy barrier. This difficulty can be alleviated by the use of biased MD simulations, as demonstrated previously for a Lennard-Jones system.[27] The application of biased MD simulations, however, is limited because the biasing parameter needs to be an explicit function of particle coordinates for the biasing force to be calculated. By contrast, biased MC simulation does not have such a limitation; therefore biasing techniques are easier to implement in MC simulations than in MD. Furthermore, MC simulation allows the use of unphysical moves, e.g., end-bridging moves,[28] to sample phase space more efficiently. This sampling efficiency is essential to equilibrate systems of complex molecules like polymer melts.

In our Monte Carlo simulations, each Monte Carlo cycle consisted of N_{beads} trial moves, where N_{beads} was the total number of beads in the system. The trial moves were randomly chosen from three types: (1) local displacement of one bead, (2) reptation of one end bead, and (3) configuration-biased re-growth[29]. These three moves were chosen with relative probabilities of 50:45:5. In addition, each Monte Carlo cycle also contained five volume change moves. The relative probabilities of all four types of Monte Carlo moves were chosen to obtain rapid equilibration, as

measured by the mean-squared displacement (MSD) of beads and decay of the chain end-to-end vector autocorrelation. The acceptance ratios for the displacement and volume change moves were both 50%, controlled through the choice of the maximum bead displacement and maximum volume change. For configuration-biased re-growth, the number of beads displaced was chosen uniformly and randomly between 1 and 8. No attempt was made to optimize the acceptance ratios of the configuration-biased re-growth or the reptation moves. Their acceptance ratios under these simulation conditions were 16% and 0.3%, respectively.

The umbrella sampling technique[30] was used to sample the free energy of formation of crystal nuclei during MC simulation. In umbrella sampling, a biasing potential energy is added to improve the sampling of configurations with small Boltzmann factors; the bias is subsequently removed during analysis of the results.

We chose a fixed biasing potential $E^{\text{bias}}(\Phi) = k_{\phi}/2(\Phi - \Phi_{\text{target}})^2$ in our free energy sampling, where Φ is the chosen reaction coordinate. The center and width of the sampling window depended on Φ_{target} and k_{ϕ}, respectively. We divided the whole sampling range $[\Phi_{\text{init}}, \Phi_{\text{final}}]$ into a series of overlapping windows. The initial configuration for each window was extracted from a MD trajectory that exhibited nucleation, such that the initial configuration had a Φ value in the corresponding window.

To implement umbrella sampling, we first carried out a sequence of m Monte Carlo moves without the biasing potential; then we calculated the value of Φ and accepted or rejected the whole sequence based on the change in the biasing potential, $\exp(-\beta\Delta E^{bias})$, where ΔE^{bias} is the difference in the biasing potential before and after the sequence:

$$\Delta E^{bias} = E^{bias}(\text{after}) - E^{bias}(\text{before}) \tag{26}$$

We used a sequence consisting of one MC cycle. In principle the biasing potential could be applied after every Monte Carlo move, but, in this case, the calculation of the reaction coordinate Φ was computationally expensive, and the value of Φ was strongly correlated from one Monte Carlo move to the next, so that the statistics could not be improved much using a shorter sequence. Sampling was performed once per sequence.

The reaction coordinate Φ was chosen to be the size of the *largest* crystal nucleus in the system, n_{max}. We divided the reaction coordinate range $0 \leq n_{max} \leq 40$ into approximately eight overlapping sampling windows and used $k_{\circ} = 0.05\ k_B T$ for all windows. In each window, an initial configuration was relaxed for $2^{16} = 65,536$ MC cycles, and then statistics were taken over a run of $2^{18} = 262,144$ MC cycles.

IV. RESULTS AND DISCUSSION

A. Determining the crystal structure

In order to test the performance of the PYS force field in the crystal phase, we prepared a system of 480 chains with the experimentally determined crystal structure[31] and equilibrated it at 200K using MD simulation. Table I compares the simulated crystal structure with the experimental one.

Being a UA force field, the PYS force field does not treat hydrogen atoms explicitly, thus resulting in a tilted hexagonal structure ($\gamma=120°$). In addition, the ordered phase generated by this force field at 200K is, in fact, a "rotator" phase [32], as shown in Fig. 1 and confirmed by the distribution of chain orientation shown in Fig. 2, rather than a perfect representation of the *n*-octane crystal. The chain orientation in Fig. 2 is defined as the azimuthal angle of a vector in the x-y plane. This vector points from the average of the projection of all odd beads on one chain on the x-y plane to that of all even beads on the same chain. Translational registry of the chain centers of mass is maintained in all three directions, which precludes this phase being a liquid crystal phase. The differences between our simulated crystal structure and the experimental one can be remedied by employing an all-atom (AA) force field[33] but not by an anisotropic united-atom model (AUA)[34]. Nevertheless, nucleation of the ordered, rotator phase is considered to be a sufficiently close approximation to that of the crystalline phase in *n*-alkanes for purposes of this study.

B. Determining the equilibrium melting point and the heat of fusion

The equilibrium melting temperature T_m is a crucial reference point for subsequent analysis of crystallization behavior. Ko *et al.*[35] used a force field similar to PYS and indirectly estimated the T_m of C400 to be within 10K of the experimental value, 410K[36].   Waheed *et al.*[19] also used the PYS force field and reported the melting of *n*-eicosane around 345K for a system with periodic boundaries, compared to the experimental value of 310K[37]. The discrepancy in Waheed's study was explained to be due in part to the superheating required to nucleate the melt phase within an essentially infinite crystal (because of the periodic boundary conditions in the simulation); in real systems, melting typically proceeds from the surface inward.

To avoid this problem, we determined T_m using a simulation with a crystal-melt interface, as proposed by Bai *et al.*[38] For this purpose, we first created a system comprising a perfect crystal of 480 chains and then increased the Lennard-Jones parameter ε for half of the system by a factor of two, effectively raising the melting point for this half of the system to some $T_m' > T_m$. Then, by trial-and-error, we chose a temperature T_1 between T_m' and T_m such that the unmodified half of the system melts, thus generating a system with a flat crystal-melt interface parallel to the (100) crystal facet. For this purpose, T_1 was set to 300K. Then all beads were restored to the original ε value, and the system was quenched to a lower temperature T_2 between 200K and 220K. (The experimental value of T_m for *n*-octane is 216.4K.) We then monitored the displacement of the crystal-melt interface at T_2 (Fig. 3).

The crystal fraction in the simulation was quantified using the global orientation order parameter P_2. An increase of the crystal domain at the expense of the melt domain is signaled by an increase of P_2, indicating that the temperature of that simulation is lower than T_m. If P_2 decreases, then the simulation temperature is higher than T_m. Thus, T_m is identified with the value of T_2 at which P_2 remains essentially unchanged with time. At each T_2, four MD simulations were performed using randomized initial velocities, with similar results. Fig. 4 shows representative trajectories at five different T_2s. Through this procedure, we determined that $T_m = 212 \pm 1K$ for n-octane using the PYS force field, which agrees well with the experimental value 216.4K.

The heat of fusion per molecule at the melting temperature is an important quantity for phase transition studies. It is calculated from

$$\Delta H_f = \Delta E + P\Delta V \text{ ,} \tag{27}$$

where the changes of energy and volume are due to the phase transformation at constant pressure and constant temperature. At constant temperature, the kinetic energy does not change, so we only measured the potential energy and average density at the simulated equilibrium melting temperature $T_m = 212K$ for crystal and melt states, respectively. These values and the average density of both crystal and melt states at several temperatures are presented in Table II. The calculation yields $\Delta H_f = 12.7 \pm 0.2$ kJ/mol. As a comparison, the value cited by Oliver $et\ al.$[7] is

ΔH_f = 20.68 kJ/mol. We attribute this difference to the fact that our simulated crystal phase is a "rotator" phase, rather than a perfect crystal phase.

C. Molecular dynamics simulation of the nucleation process

Having determined the equilibrium melting temperature T_m, we performed MD simulations to study crystal nucleation in n-octane melts. First the system was equilibrated in the melt state at 250K for 1 ns; then it was quenched to 170K, which is about 20% supercooling. In a typical trajectory after quenching (Fig. 5), three time periods can be observed: (i) an initial period from $t = 0$ to 2 ns, during which the potential energy decreases rapidly to re-establish equipartition of energy after the quench; (ii) an induction period from $t = 2$ to 31 ns, during which the system is metastable and there is no evidence of a nucleation event; and (iii) a period of crystal growth after a nucleation event occurs ($t > 31$ ns). Around $t = 28$ ns, a nucleus with n ~ 27 apparently forms but is short-lived. Around $t = 31$ ns, another nucleus forms that grows rapidly to a size of n ~ 25 and then serves as the object from which the rest of the system crystallizes. This observation is consistent with the picture of classical nucleation theory. As demonstrated below, the top of the free energy barrier is relatively flat, and there is a finite probability that any particular nucleus of size comparable to the critical value, n^*, will either re-cross the barrier and melt or else proceed to form a stable crystal phase. The onset of nucleation is clearly represented by a sudden increase of n_{max}, whereas overall density, potential energy,

P_2, and P_{trans} are all less sensitive to the nucleation event and show delayed response to nucleation.

In order to evaluate how the nucleus definition influences this result, we re-analyzed the same MD trajectory using two additional sets of cutoffs in Esselink's nucleus definition, i.e., ($\theta_c = 15°$, $r_c = 1.8\sigma$) and ($\theta_c = 5°$, $r_c = 1.3\sigma$) (Fig. 6). The n_{max} curve with cutoffs ($\theta_c = 5°$, $r_c = 1.3\sigma$) displays considerable fluctuation after the nucleation event occurs, at around 32 ns; this fluctuation suggests that the size of a nucleus is overly sensitive to small motions at its surface, and that the nucleus definition is too restrictive. On the other hand, the n_{max} curve with cutoffs ($\theta_c = 15°$, $r_c = 1.8\sigma$) displays "spikes" after the nucleation occurs, which we trace to the "merger" and subsequent "splitting" of two different nuclei; thus, this nucleus definition is too lenient. Therefore we confirmed ($\theta_c = 10°$, $r_c = 1.5\sigma$) to be a good empirical choice for the nucleus definition for purpose of our study.

In all, we performed 48 independent MD simulations for a system of 480 chains and 24 independent MD simulations for a system of 960 chains, each quenched from 250K to 170K at time $t = 0$. The systems with 480 chains were simulated for 60 ns; 30 of the 48 simulations exhibited nucleation, as typified by Fig. 5. The systems with 960 chains were simulated for 30 ns; 20 of the 24 simulations exhibited nucleation.

Wedekind *et al.*'s method[16] was used to estimate the critical nucleus size n^* and the average induction time τ^*. The results are $n^* = 19$ and $\tau^* = 24 \pm 12$ ns for a system of 480 chains, and $n^* = 21$ and $\tau^* = 16 \pm 10$ ns for a system of 960 chains. Fig. 7 illustrates how to estimate n^* and τ^* through a fit of Eq. (25) to the MFPT of n_{max}, $\tau(n_{max})$. Fig. 7 shows a large statistical error in $\tau(n_{max})$ for $n_{max} > n^*$; this error is due to the limited number of MD trajectories used for averaging. Moreover, some MD simulations failed to exhibit nucleation throughout their whole simulation time, so τ^* is underestimated, more so for the system of 480 chains than for the system of 960 chains because the former has a higher percentage of simulations that failed to exhibit nucleation. Therefore, the induction time τ^* estimated for a system of 960 chains is more reliable.

The induction time τ^* is equal to the inverse of the product of the nucleation rate I and the volume of the system V:

$$\tau^* = (I \times V)^{-1}. \qquad (28)$$

Plugging $\tau^* = 16 \pm 10$ ns into Eq. (28), we obtain a nucleation rate I equal to $(2.7 \pm 0.6) \times 10^{26}$ cm^{-3}sec^{-1} for a system of 960 chains at 170K, where the system volume is calculated from the melt state density in Table II. We further calculate the critical free energy ΔG^* using Eq. (17), where the kinetic prefactor I_0 was calculated by Uhlmann *et al.* to be 3.71×10^{32} cm^{-3}sec^{-1}.[8] The calculated critical free energy ΔG^* is $14.1 \pm 0.4\ k_BT$ for a system of 960 chains at 170K. However, this value of ΔG^* should be treated with caution because it is hard to determine I_0 precisely.

Uhlmann *et al.* calculated I_0 using Eq. (18)-(19), an approximation that is good for molecules of isotropic shape, e.g., fused salts, metals, and simple organic liquids. However, the *n*-octane molecule is anisotropic, and only those molecules that reach the nucleus surface with certain orientations contribute to effective attachment. Therefore I_0 is overestimated by Eq. (18)-(19), and thus ΔG^* is also overestimated. It is desirable, then, to employ another simulation method from which one can calculate the critical free energy ΔG^* directly, without having to invoke additional assumptions or approximations.

D. Monte Carlo sampling of the nucleation free energy barrier

The free energy of formation, or reversible work, of a *n*-sized nucleus, $\Delta G(n)$, can be calculated from the equilibrium nucleus size distribution, as follows:[15]

$$\Delta G(n)/k_B T = -\ln N(n)/N_c + const. \tag{29}$$

where $N(n)$ is the number of *n*-sized nuclei observed during the simulation, and N_c is the total number of sites in the system on which nuclei can form, which is equal to the total number of chains in the system. Because a 1-sized nucleus correspond to a molecule in the melt state, the constant in Eq. (29) can be determined by equating $\Delta G(n=1)$ to zero.

For sufficiently small values of *n*, multiple nuclei of various *n* are observed to form spontaneously within a system of finite size. For larger values of *n,* especially those approaching the critical size *n**, umbrella sampling is required to ensure adequate

statistics for estimating the relative probabilities of these nuclei. In general, only one nucleus of size n_{max} is observed in each of the biased simulations, and n_{max} is well separated from those small values of n where multiple nuclei spontaneously occur. Thus, within a given simulation in which umbrella sampling is used, we can approximate the differences in free energy for nuclei of different sizes using Eq. (29), replacing n by n_{max} and N_c by the number of systems sampled. Simulations with different biases are chosen to ensure overlapping ranges of n_{max}, so that all of the free energy curves can be shifted subsequently to form a single, continuous, universal curve of $\Delta G(n)$ vs n. In this way, we constructed the whole free energy curve without loss of accuracy. We have checked this approach by reproducing an Ising model nucleation simulation by Chandler et al.[14]

Fig. 8 shows $\Delta G(n)$ versus n at 170K. In order to evaluate the finite size effect, we present the results for systems of 480 chains and 960 chains. The nucleation free energy curve does not change with system size, indicating that a system of 480 n-octane chains is sufficiently large to be free from finite size effects under these simulation conditions.

From the critical free energy ΔG^* obtained by Monte Carlo and the nucleation rate I reported above from MD simulations, both at 170K, we determined the kinetic prefactor I_0 using Eq.(17), to be $I_0 = (2.95 \pm 3.61) \times 10^{30}$ cm^{-3}sec^{-1}. This is about two orders of magnitude lower than the value estimated by Uhlmann et al. using Eq (18)-(19). Since I_0 is only weakly temperature-dependent, we can use this I_0 to estimate

the nucleation rate at other temperatures, if the critical free energy ΔG^* for those temperatures is known. This is particularly valuable for temperatures close to the melting point, where brute-force MD simulations are too inefficient to study the nucleation event directly.

Similar free energy sampling has been performed at 180K and 190K. The critical nucleus size n^* and the critical free energy ΔG^* for an n-octane melt at 170K, 180K, and 190K, obtained from the maxima in the curves for G/k_BT vs n, are summarized in Table III. At 170K, the critical nucleus size obtained by MC is in reasonable agreement with that indicated by the MD results. As the supercooling ΔT decreases toward zero, both the critical size n^* and the critical free energy ΔG^* increase, which is consistent with classical nucleation theory. We did not observe a free energy barrier at 190K, probably because ΔT was so small. In this case, the critical nucleus may have been too big for our finite-size system.

The crystal-liquid interfacial free energy σ of n-octane has been calculated by Uhlmann et $al.$[8] and by Oliver et $al.$[7] from their experimental measurements of nucleation rate at $\Delta T/T_m$ values of 0.111 and 0.138, respectively. By assuming a spherical nucleus model, they estimated σ to be between 10.3 and 13.4 mJ/m^2. We also used the spherical nucleus model to calculate σ from the ΔG^* determined by Monte Carlo simulation, using Eq.(5), and obtained a value for σ of 12.0 mJ/m^2 at 170K. The values of T_m and ΔH_f in Eq. (5) both come from our MD simulations, reported in Section B above. The σ determined in this way from the simulation data

is consistent with the experimental studies. The free energy curves of the spherical nucleus model are shown in Fig. 9, and illustrate the sensitivity of the critical free energy to the value of surface energy.

Although the spherical nucleus model can be used to calculate an interfacial free energy σ from the critical free energy ΔG^*, the shape of the free energy curve deviates from the simulation data significantly (Fig. 9). Visual inspection of nuclei indicates that the spherical model is a poor description of the actual nuclei for n-octane. Fig. 10 is a snapshot of a crystal nucleus containing 18 n-octane chains at 170K; its shape is more cylindrical than spherical. Furthermore, the critical nucleus size n^* calculated from ΔG^* based on Eq. (11) is significantly smaller than the n^* measured in simulation, proving that the spherical nucleus model is not an appropriate model for the n-octane crystal nuclei.   Because the variable-length cylinder model also has to satisfy Eq. (11), we conclude that neither the spherical nucleus model nor the variable-length cylindrical nucleus model describes the crystal nucleus of n-octane chains well.

Therefore we turn to the fixed-length cylinder model. The length of an extended n-octane molecule l_0 is 0.82 nm. Applying Eq. (16a)-(16b), we obtain the interfacial free energy of the end surface $\sigma_e = 5.4$ mJ/m^2 and of the side surface $\sigma_s = 6.8$ mJ/m^2 at 170K. Using these free energy values, the fixed-length cylinder model fits our simulation data well over the whole range of n (Fig. 9). Similarly, the interfacial free energies at 180K and 190K are calculated (Table IV). Although we did not observe

any critical nuclei at 190K, we can still parameterize the fixed-length cylinder model, Eq. (13), to match the pre-critical part of the simulated free energy curve and to obtain the interfacial free energies. The interfacial free energies at 190K predict a critical nucleus size n^* of about 113, which is too big to observe reliably in our system of only 960 chains. The fixed-length cylindrical nucleus model captures quantitatively the formation of a crystal nucleus in the n-octane system for all three supercooling temperatures (Fig. 11).

As ΔT decreases toward zero, the interfacial free energy does not change much for the side surface; however, it decreases significantly for the end surface. This difference is attributed to the longitudinal chain motion, which increases dramatically with increasing temperature; the transverse chain motion is not sensitive to temperature. This temperature dependence of chain mobility is consistent with previous observations by Ryckaert *et al.*[32]

V. CONCLUSIONS

In this paper, we have studied homogeneous nucleation of the crystal phase from an n-octane melt, using both MD and MC methods. For the first time, the critical nucleus of a chain molecule system was identified, both kinetically using an unbiased MD method and analysis of mean first passage times, and thermodynamically using the MC method with umbrella sampling. The results of both methods are in reasonable agreement with each other and with the available experimental data. Within the framework of the classical nucleation theory, a cylindrical nucleus model

provides a reliable description of the dependence of free energy on nucleus size, $\Delta G(n)$. It allows us to estimate the critical nucleus size even at small degrees of supercooling, from simulation results for pre-critical nuclei, and to calculate the solid-liquid interfacial free energies for both the end-surface and side-surface of the nucleus. The decoupling of these two surfaces is important to understand the crossover from extended chain nucleation to folded chain nucleation in chain molecule systems.

Homogeneous nucleation of the crystal phase from a quiescent melt of mono-disperse short chains represents an idealized case. However, we believe that the concepts and methods employed in this study can be extended to study more complicated nucleation behavior typical of longer chains, e.g., integer-folded nucleation and flow-induced nucleation, because the properties of the critical nucleus should also be the controlling factors therein.

Acknowledgements

References

[1] K. F. Kelton. (Academic, Boston, 1991).

[2] D. W. Oxtoby, Journal of Physics: Condensed Matter **4** (38), 7627 (1992).

[3] G. Strobl, The European Physical Journal E: Soft Matter and Biological Physics **3** (2), 165 (2000); M. Muthukumar and P. Welch, Polymer **41** (25), 8833 (2000); P. D. Olmsted, W. C. K. Poon, T. C. B. McLeish, N. J. Terrill, and A. J. Ryan, Physical Review Letters **81** (2), 373 (1998); G. Allegra and S. V. Meille, Physical Chemistry Chemical Physics **1** (22), 5179 (1999).

[4] E. B. Sirota and D. M. Singer, The Journal of Chemical Physics **101** (12), 10873 (1994); G. Ungar, J. Stejny, A. Keller, I. Bidd, and M. C. Whiting, Science **229** (4711), 386 (1985).

[5] D. Turnbull and R. L. Cormia, The Journal of Chemical Physics **34** (3), 820 (1961); H. Kraack, M. Deutsch, and E. B. Sirota, Macromolecules **33** (16), 6174 (2000); G. Eder, H. Janeschitz-Kriegl, and S. Liedauer, Progress in Polymer Science **15** (4), 629 (1990); H. Janeschitz-Kriegl, E. Ratajski, and H. Wippel, Colloid & Polymer Science **277** (2), 217 (1999); H. Janeschitz-Kriegl, E. Ratajski, and M. Stadlbauer, Rheologica Acta **42** (4), 355 (2003).

[6] R. L. Cormia, F. P. Price, and D. Turnbull, The Journal of Chemical Physics **37** (6), 1333 (1962).

[7] M. J. Oliver and P. D. Calvert, Journal of Crystal Growth **30** (3), 343 (1975).

[8] D. R. Uhlmann, G. Kritchevsky, R. Straff, and G. Scherer, The Journal of Chemical Physics **62** (12), 4896 (1975).

[9] H. Takeuchi, The Journal of Chemical Physics **109** (13), 5614 (1998); H. Meyer and F. Muller-Plathe, Macromolecules **35** (4), 1241 (2002); T. Yamamoto, The Journal of Chemical Physics **115** (18), 8675 (2001); R. H. Gee and L. E. Fried, The Journal of Chemical Physics **118** (8), 3827 (2003); S. Fujiwara and T. Sato, Physical Review Letters **80** (5), 991 (1998).

[10] K. Esselink, P. A. J. Hilbers, and B. W. H. van Beest, The Journal of Chemical Physics **101** (10), 9033 (1994).

[11] T. Miura, R. Kishi, M. Mikami, and Y. Tanabe, Physical Review E **63** (6), 061807 (2001).

[12] J. S. van Duijneveldt and D. Frenkel, The Journal of Chemical Physics **96** (6), 4655 (1992); P. R. ten Wolde, M. J. Ruiz-Montero, and D. Frenkel, The Journal of Chemical Physics **104** (24), 9932 (1996); P.-R. t. Wolde, M. J. Ruiz-Montero, and D. Frenkel, Faraday Discussions **104**, 93 (1996); I. Kusaka, Z. G. Wang, and J. H. Seinfeld, Journal of Chemical Physics **108** (9), 3416 (1998); S. Wonczak, R. Strey, and D. Stauffer, The Journal of Chemical Physics **113** (5), 1976 (2000); R. Radhakrishnan and B. L. Trout, The Journal of Chemical Physics **117** (4), 1786 (2002); G. O. Berim and E. Ruckenstein, The Journal of Chemical Physics **117** (16), 7732 (2002); P. Beaucage and N. Mousseau, Physical Review B (Condensed Matter and Materials Physics) **71** (9), 094102 (2005); J.-M. Leyssale, J. Delhommelle, and C. Millot, The Journal of Chemical Physics **122** (10), 104510 (2005); K. Brendel, G. T. Barkema, and H. van Beijeren, Physical Review E

(Statistical, Nonlinear, and Soft Matter Physics) **71** (3), 031601 (2005); S. Punnathanam and P. A. Monson, The Journal of Chemical Physics **125** (2), 024508 (2006); H. Wang, H. Gould, and W. Klein, Physical Review E (Statistical, Nonlinear, and Soft Matter Physics) **76** (3), 031604 (2007).

13 J. H. ter Horst and D. Kashchiev, The Journal of Chemical Physics **119** (4), 2241 (2003); L. S. Bartell and D. T. Wu, The Journal of Chemical Physics **125** (19), 194503 (2006).

14 A. C. Pan and D. Chandler, J. Phys. Chem. B **108** (51), 19681 (2004).

15 S. Auer and D. Frenkel, The Journal of Chemical Physics **120** (6), 3015 (2004).

16 J. Wedekind, R. Strey, and D. Reguera, The Journal of Chemical Physics **126** (13), 134103 (2007).

17 M. G. Broadhurst, Journal of Research of the National Bureau of Standards - A. Physics and Chemistry **66A**, 241 (1962).

18 W. Paul, D. Y. Yoon, and G. D. Smith, The Journal of Chemical Physics **103** (4), 1702 (1995).

19 N. Waheed, M. S. Lavine, and G. C. Rutledge, The Journal of Chemical Physics **116** (5), 2301 (2002).

20 N. Waheed, M. J. Ko, and G. C. Rutledge, Polymer **46** (20), 8689 (2005).

21 V. A. Harmandaris, V. G. Mavrantzas, and D. N. Theodorou, Macromolecules **31** (22), 7934 (1998); V. G. Mavrantzas and D. N. Theodorou, Macromolecules **31** (18), 6310 (1998).

22 W. Smith and T. R. Forester, Journal of Molecular Graphics **14** (3), 136 (1996).

23 S. Plimpton, Journal of Computational Physics **117** (1), 1 (1995); (Sandia National Laboratory), Vol. 2009.

24 M. S. Lavine, N. Waheed, and G. C. Rutledge, Polymer **44** (5), 1771 (2003).

25 W. Paul, G. D. Smith, and D. Y. Yoon, Macromolecules **30** (25), 7772 (1997).

26 D. Kashchiev, The Journal of Chemical Physics **127** (6), 064505 (2007).

27 J. M. Leyssale, J. Delhommelle, and C. Millot, Chemical Physics Letters **375** (5-6), 612 (2003).

28 P. V. K. Pant and D. N. Theodorou, Macromolecules **28** (21), 7224 (1995).

29 J. I. Siepmann, Molecular Physics **70** (6), 1145 (1990).

30 G. M. Torrie and J. P. Valleau, Chemical Physics Letters **28** (4), 578 (1974).

31 N. Norman and H. Mathisen, Acta Chemica Scandinavica **15** (8), 1747 (1961); H. Mathisen, N. Norman, and B. F. Pedersen, Acta Chemica Scandinavica **21** (1), 127 (1967).

32 J. P. Ryckaert, M. L. Klein, and I. R. Mcdonald, Physical Review Letters **58** (7), 698 (1987); J. P. Ryckaert, I. R. Mcdonald, and M. L. Klein, Molecular Physics **67** (5), 957 (1989).

33 J. M. Polson and D. Frenkel, The Journal of Chemical Physics **111** (4), 1501 (1999).

34 S. Toxvaerd, The Journal of Chemical Physics **93** (6), 4290 (1990); S. Toxvaerd, The Journal of Chemical Physics **107** (13), 5197 (1997).

35 M. J. Ko, N. Waheed, M. S. Lavine, and G. C. Rutledge, The Journal of Chemical Physics **121** (6), 2823 (2004).

36 G. M. Stack, L. Mandelkern, and I. G. Voigt-Martin, Macromolecules **17** (3), 321 (1984).

[37]   H. Kraack, E. B. Sirota, and M. Deutsch, The Journal of Chemical Physics **112** (15), 6873 (2000).
[38]   X.-M. Bai and M. Li, The Journal of Chemical Physics **124** (12), 124707 (2006).
[39]   W. Humphrey, A. Dalke, and K. Schulten, Journal of Molecular Graphics **14** (1), 33 (1996).

Table I. Crystal structure of *n*-octane at 200K.

Crystal structure[*]	**Experiments**	**MD simulation**
Crystal structure[*]	Triclinic	Triclinic
a (nm)[*]	0.422 ± 0.002	0.47 ± 0.003
b (nm)	0.479 ± 0.002	0.47 ± 0.003
c (nm)	1.102 ± 0.002	1.226 ± 0.005
α (degree)	94.7 ± 0.3	81.7 ± 1.0
β (degree)	84.3 ± 0.3	101.1 ± 1.0
γ (degree)	105.8 ± 0.3	120.0 ± 1.0
density (g/cm^3)	0.858	0.826 ± 0.003

[*]: a, b, c, α, β, γ are lattice constants of a triclinic crystal.

Table II. Potential energy per chain and average density of *n*-octane systems at pressure $P = 1$ atm and several different temperatures.

T (K)	potential energy per chain (kJ/mol)		average density (g/cm^3)	
	crystal state	melt state	crystal state	melt state
212	-37.60 ± 0.34	-24.86 ± 0.34	0.818 ± 0.003	0.745 ± 0.003
190	-40.68 ± 0.28	-28.17 ± 0.30	0.831 ± 0.003	0.760 ± 0.003
180	-41.92± 0.26	-29.83 ± 0.29	0.836 ± 0.003	0.767 ± 0.003
170	-43.09± 0.24	-31.59 ± 0.32	0.840 ± 0.003	0.775 ± 0.003

Table III. The crystal nucleation free energy as a function of nucleus size n for an n-octane melt containing 960 chains.

T (K)	$\Delta T/T_\mathrm{m}$	n^*	ΔG^* ($k_\mathrm{B}T$)
170	19.8%	18 ± 3	9.3 ± 1.0
180	15.1%	23 ± 3	12.5 ± 1.0
190	10.4%	*	*

_____

[*]: We did not observe a critical nucleus in simulations at 190K.

Table IV. Crystal-liquid interfacial free energy of *n*-octane molecules.

T (K)	σ_e (mJ/m^2)	σ_s (mJ/m^2)
170	5.4 ± 0.5	6.8 ± 0.7
180	3.3 ± 0.3	8.4 ± 0.8
190	2.9 ± 0.3	8.0 ± 0.8

Figure Captions:

Figure 1: A snapshot of 480 *n*-octane chains simulated at 200K. (a) viewed along the *a*-axis of the triclinic unit cell; (b) viewed along the *b*-axis of the triclinic unit cell; (c) viewed along chain direction. This figure was rendered by VMD.[39]

Figure 2: The chain orientation distribution for a system of 480 *n*-octane chains at 200K in the rotator phase. The chain orientation is defined as the azimuthal angle of a vector in the x-y plane. This vector points from the average of the projection of all odd beads on one chain on the x-y plane to that of all even beads on the same chain.

Figure 3: Determination of the equilibrium melting temperature with a crystal-melt interface. 480 *n*-octane chains are rendered as line models. Boundaries are periodic in all three directions. Two periodic images in the horizontal direction are shown to emphasize more clearly the interfaces between the amorphous melt and ordered crystalline regions. (a) at T = 210K, the interface moves toward the melt region; (b) at T=212K, the interface stays stationary for at least 3 ns; (c) at T = 214K, the interface moves toward the crystalline region, and melting of the crystal can be seen. This figure was rendered by VMD.[39]

Figure 4: Global orientation order parameter P_2 as a function of time at five different temperatures, for a system of 480 *n*-octane chains with a crystal-melt interface. Within the precision achievable in 3 ns, the equilibrium melting temperature T_m is 212 ± 2K.

Figure 5: Evolution of characteristic variables for a system of 960 n-octane chains during a typical MD simulation, after quenching from 250K to 170K at t = 0. (a) potential energy and volume per chain; (b) size of the largest nucleus, n_{max}, and the global orientation order parameter, P_2; (c) fraction of *trans* states, P_{trans}.

Figure 6: The maximum nucleus size n_{max} as a function of time, using three different sets of cutoff angle and cutoff radius in Esselink's definition of nucleus[10]. Vertical offsets were made for purposes of clarity.

Figure 7: The mean first passage time (MFPT) of maximum nucleus size n_{max} from 24 MD simulations of a system of 960 n-octane chains quenched from 250K to 170K at $t =$ 0. The open circles are simulation data, and the solid line is the formula of Eq. (19), with n^*, τ^* and b parameterized to fit the simulation data.

Figure 8: The free energy of formation for a crystal nucleus in a melt of n-octane chains at 170K. System with 480 chains (stars); system with 960 chains (open circles). In both cases the critical nucleus size is 18 chains and the free energy barrier height is 9.3 ± 1.0 $k_B T$.

Figure 9: The free energy of formation for a crystal nucleus in a melt of 960 n-octane chains at 170K. Simulation data (filled circles); spherical nucleus model using surface free energy σ of Uhlmann *et al.*[8] (triangles); spherical nucleus model using surface free

energy σ of Oliver et $al.$[7] (inverted triangle); spherical nucleus model fit using surface free energy σ = 12.0 mJ/m^2, chosen to match the critical nucleus free energy from simulation (dashed curve); cylindrical nucleus model using surface free energies σ = 5.4 mJ/m^2 for the end surface and σ = 6.8 mJ/m^2 for the lateral surface, chosen to fit both the critical nucleus free energy and the critical nucleus size of the simulation data (solid curve).

Figure 10: A snapshot of a crystal nucleus thatconsists of 18 n-octane chains from a Monte Carlo simulation of a melt of 960 n-octane chains at 170K. (a): side view; (b): top view. This figure was rendered by VMD.[39]

Figure 11: The free energy of formation for a crystal nucleus in a melt of 960 n-octane chains at 170K, 180K, and 190K, respectively. Simulation data (open symbols); fixed length cylindrical nucleus model using Eq.(12) (solid curves). The values of the interfacial free energy σ_s and σ_e used in generating the modeled curves are presented in Table IV.

(a)　　　　　(b)　　　　　(c)
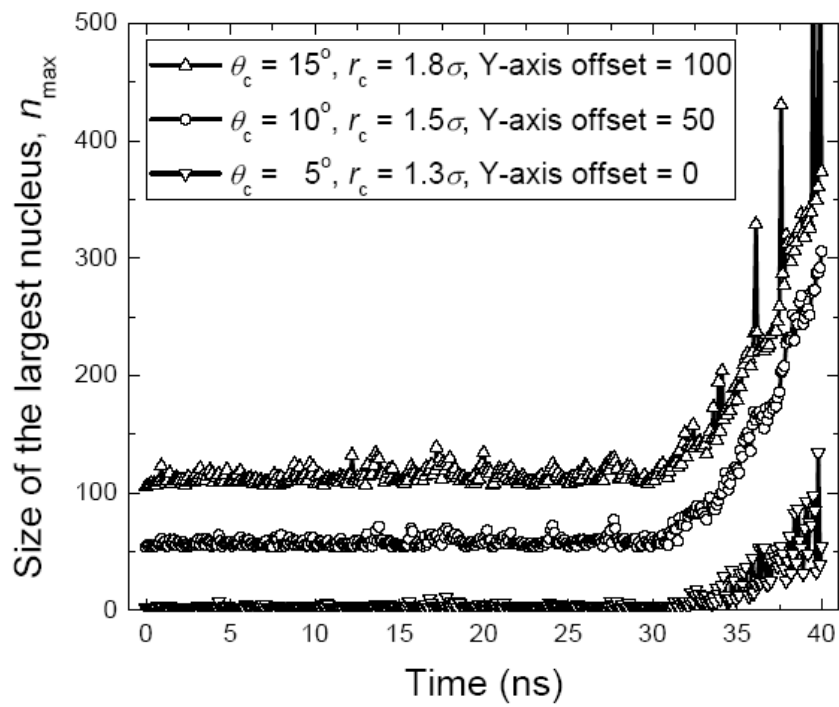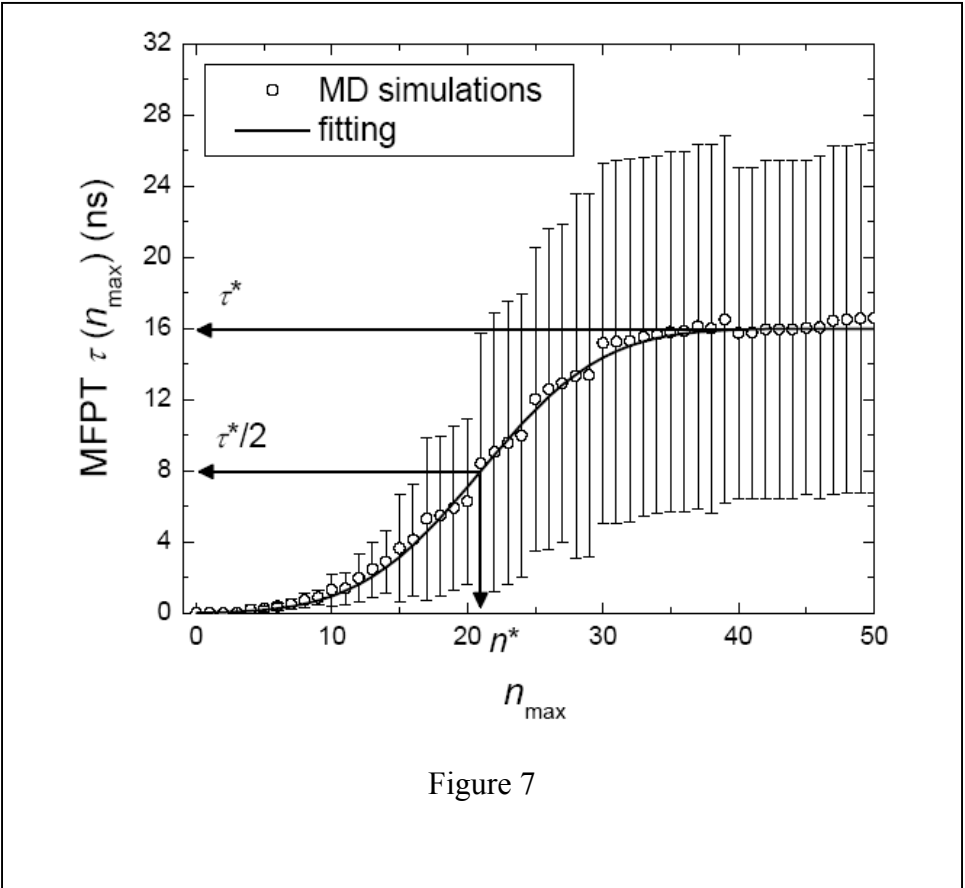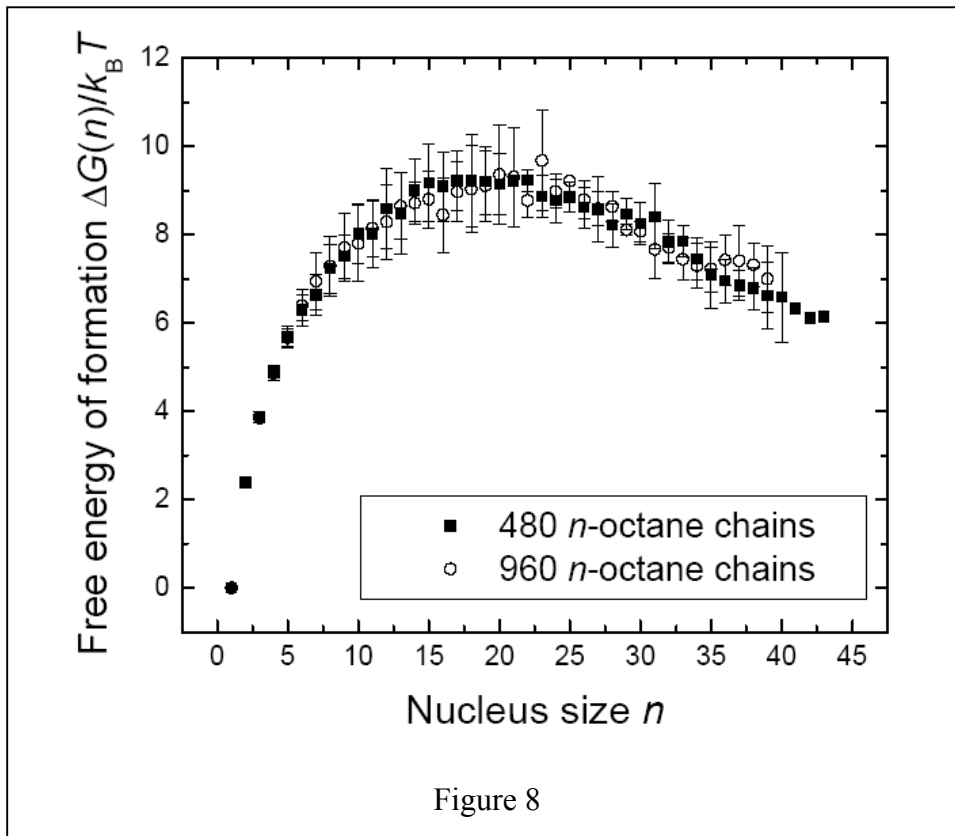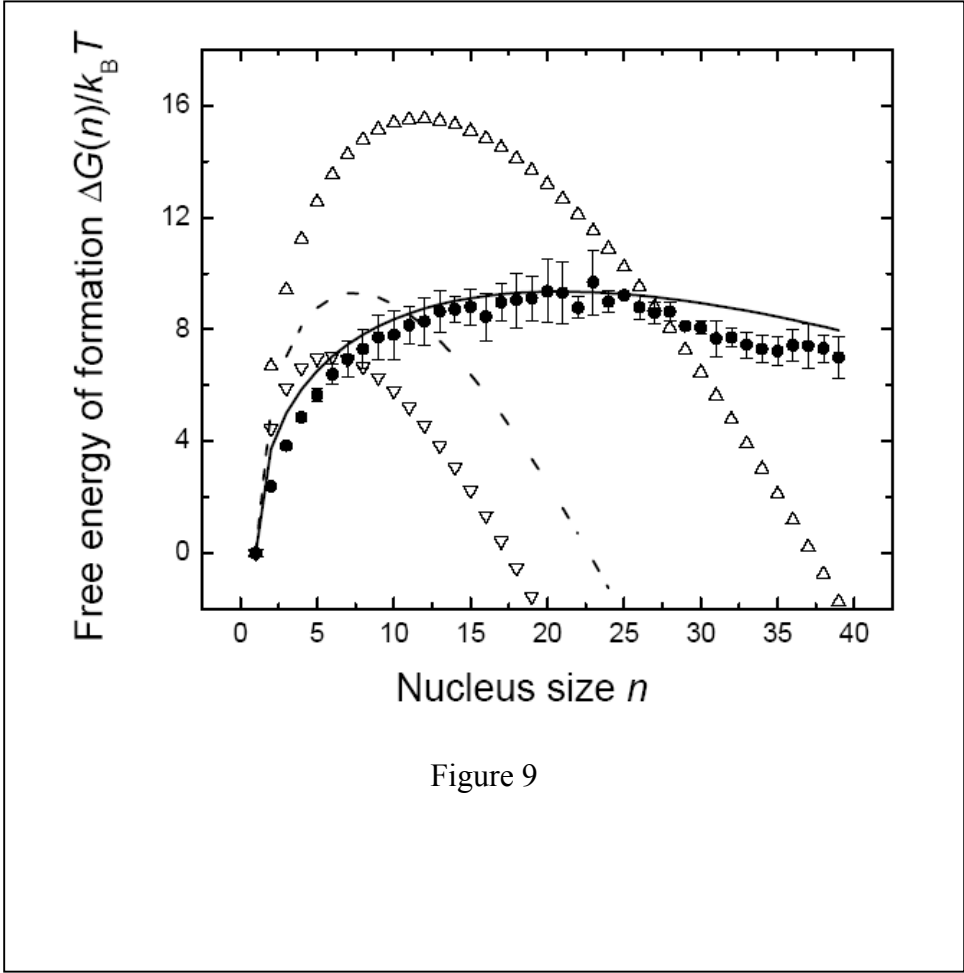
Figure 1
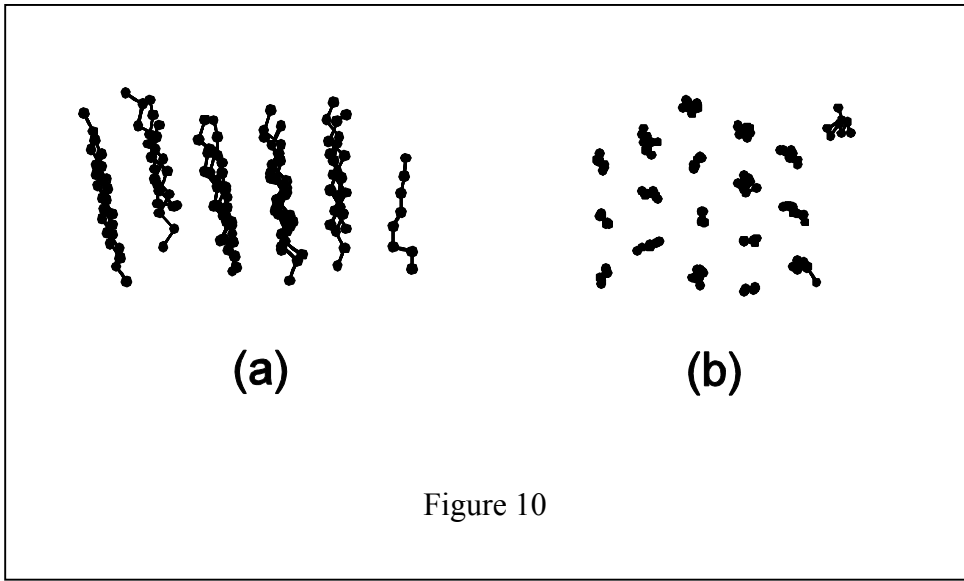
Figure 2

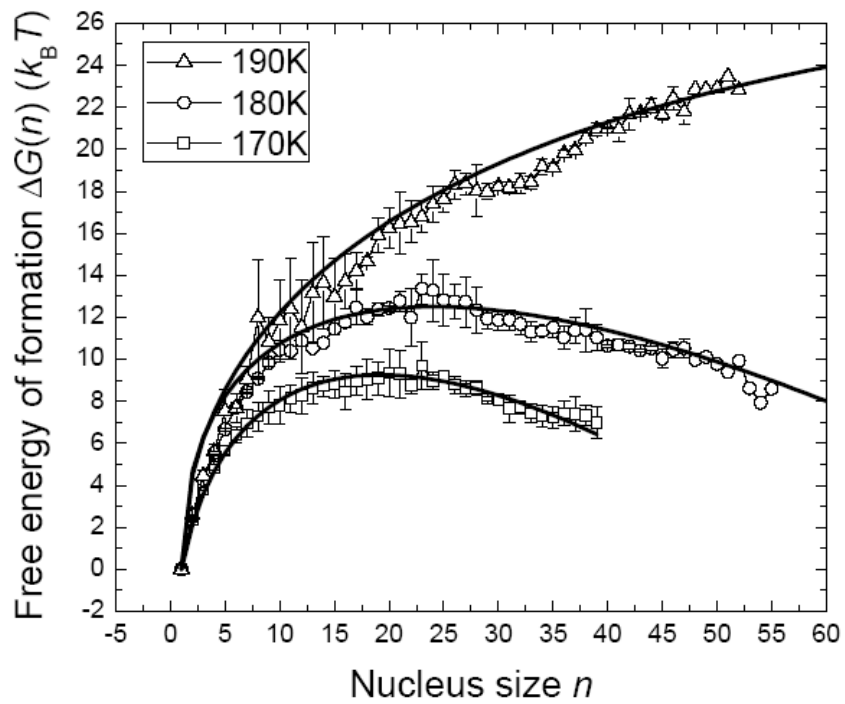(a)

(b)

(c)
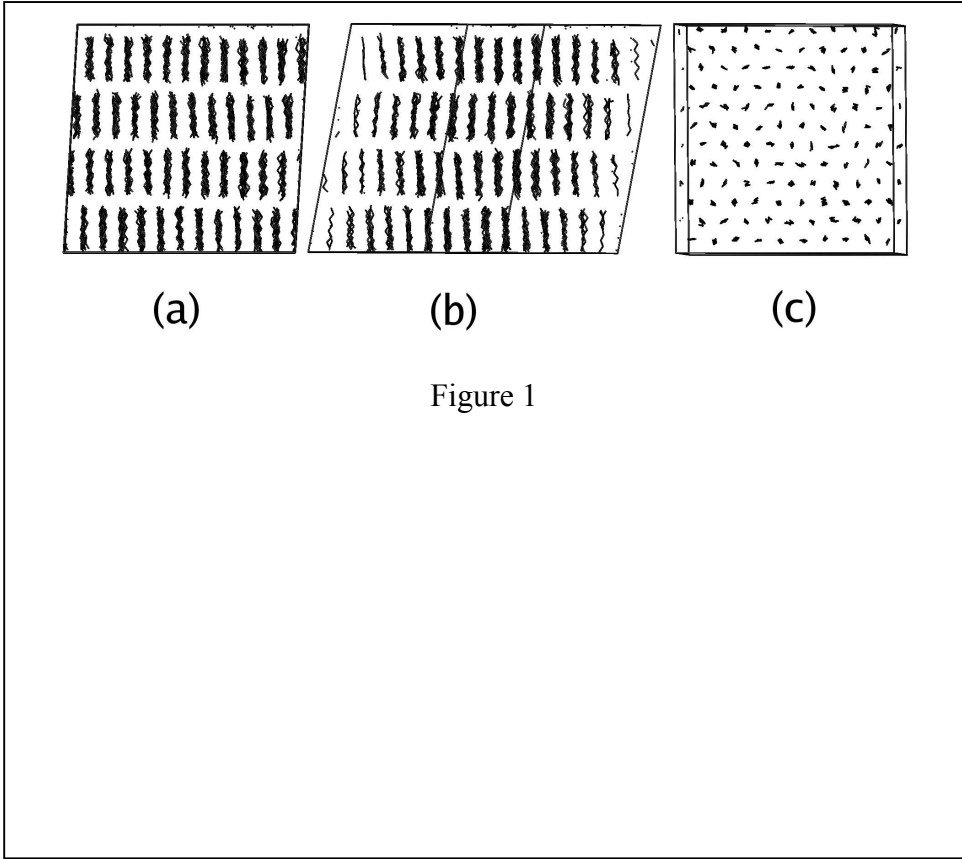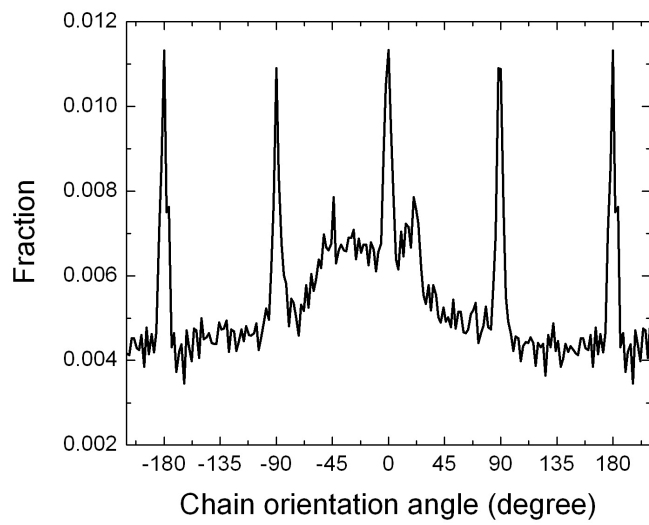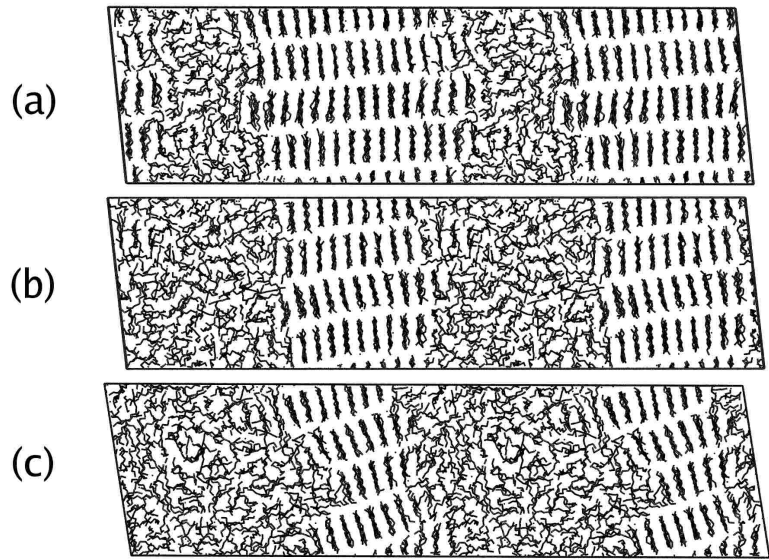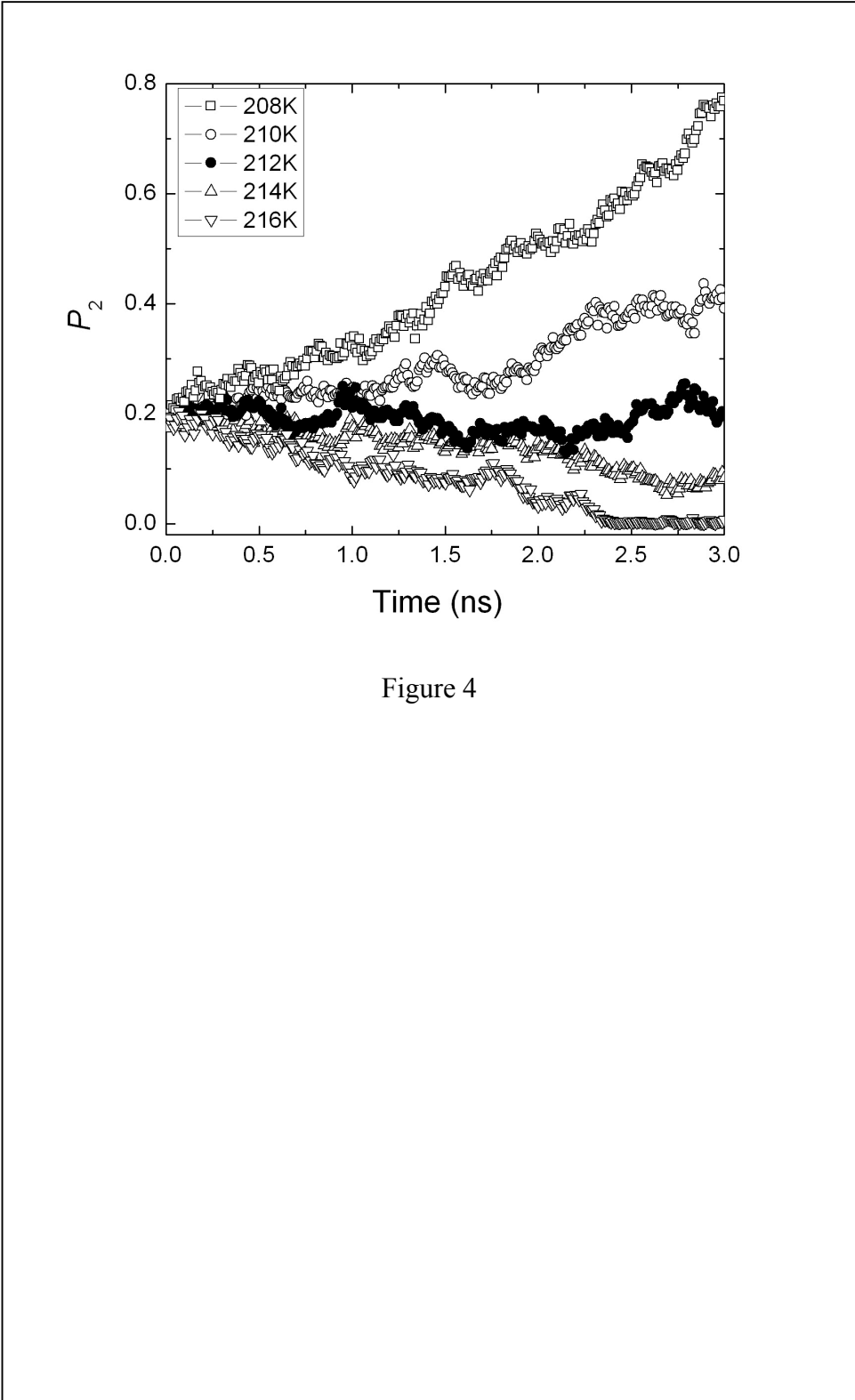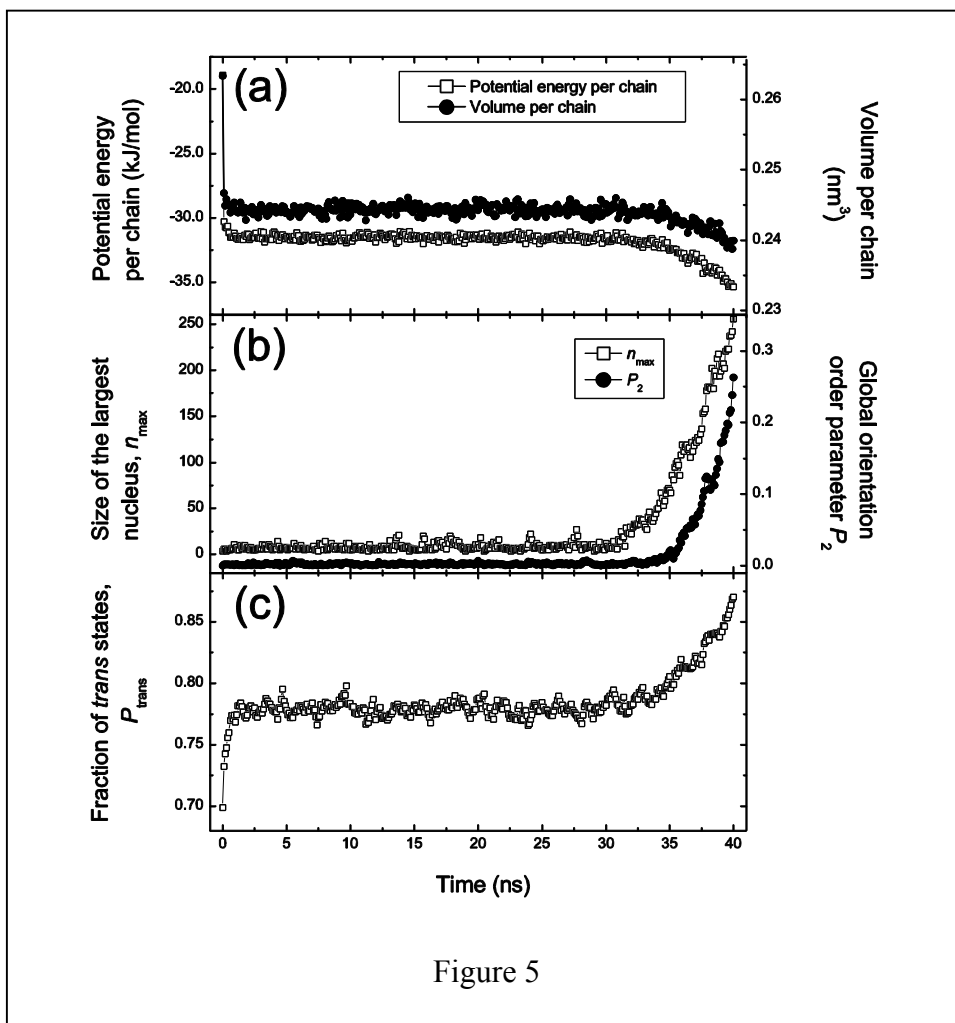
Figure 3

Figure 4

Figure 5

Figure 6

Figure 7

Figure 8

Figure 9

Figure 10

Figure 11